

Type Ia supernova ejecta-donor interaction: explosion model comparison

C. McCutcheon,^{1,2,3} Y. Zeng,^{1,2,4} Z.-W. Liu,^{1,2}* R. G. Izzard,³† K.-C. Pan,⁵‡ H.-L. Chen,^{1,2} and Z. Han^{1,2,4}

¹*Yunnan Observatories, Chinese Academy of Sciences (CAS), Kunming 650216, P.R. China*

²*Key Laboratory for the Structure and Evolution of Celestial Objects, CAS, Kunming 650216, P.R. China*

³*Astrophysics Research Group, Faculty of Engineering and Physics, University of Surrey, Guildford, GU2 7XH, United Kingdom*

⁴*University of Chinese Academy of Sciences, Beijing 100049, China*

⁵*Department of Physics and Institute of Astronomy, National Tsing Hua University, Hsinchu 30013, Taiwan, R.O.C.*

Accepted XXX. Received YYY; in original form ZZZ

ABSTRACT

In the single-degenerate scenario of Type Ia supernovae (SNe Ia), the interaction between high-speed ejected material and the donor star in a binary system is expected to lead to mass being stripped from the donor. A series of multi-dimensional hydrodynamical simulations of ejecta-donor interaction have been performed in previous studies most of which adopt either a simplified analytical model or the W7 model to represent a normal SN Ia explosion. Whether different explosion mechanisms can significantly affect the results of ejecta-donor interaction is still unclear. In this work, we simulate hydrodynamical ejecta interactions with a main-sequence (MS) donor star in two dimensions for two near-Chandrasekhar-mass explosion models of SNe Ia, the W7 and N100 models. We find that about 0.30 and 0.37 M_{\odot} of hydrogen-rich material are stripped from a 2.5 M_{\odot} donor star in a 2 day orbit by the SN Ia explosion in simulations with the W7 deflagration and N100 delayed-detonation explosion model, respectively. The donor star receives a kick of about 74 and 86 km s^{-1} , respectively, in each case. The modal velocity, about 500 km s^{-1} , of stripped hydrogen-rich material in the N100 model is faster than the W7 model, with modal velocity of about 350 km s^{-1} , by a factor 1.4. Based on our results, we conclude that the choice of near-Chandrasekhar-mass explosion model for normal SNe Ia seems to not significantly alter the ejecta-donor interaction for a given main-sequence donor model, at least in 2D.

Key words: binaries: close – supernovae: general – methods: numerical

1 INTRODUCTION

Type Ia supernovae (SNe Ia) are widely believed to be thermonuclear explosions of carbon-oxygen white dwarfs (CO WDs, Hoyle & Fowler 1960). As a class, they exhibit remarkable homogeneity in light-curves and are extremely luminous, making them ideal candidates to be used as standard candles for distance measurement on an universal scale. This property was notably used to first measure the accelerating expansion of the universe (Riess et al. 1998; Schmidt et al. 1998; Perlmutter et al. 1999). They are also important contributors to the abundance of heavy elements and therefore chemical evolution in their host galaxies, making the subject of their progenitor systems of great importance in the field. However, there has been much debate over the nature of their progenitor systems in trying to explain the variation in observed properties, leading to a range of potential progenitor models. For instance, the single-degenerate (SD) scenario (Whelan & Iben 1973), the double-degenerate (DD) scenario (Iben & Tutukov 1984; Webbink 1984; Pakmor et al. 2010)

and the sub-Chandrasekhar double-detonation scenario (Taam 1980; Fink et al. 2007; Shen et al. 2010; Sim et al. 2010; Woosley & Kasen 2011; Gronow et al. 2020) have been proposed for producing SNe Ia. In addition, the exact explosion mechanism of SNe Ia remains unclear, although they are accepted to be thermonuclear explosions of WDs in binary systems (Hillebrandt et al. 2013; Maoz et al. 2014).

The SD and the DD scenarios have been widely studied over the past decades. In the DD scenario, two WDs with total mass $\geq M_{\text{Ch}} \sim 1.4 M_{\odot}$ merge because of gravitational wave emission in a binary or possibly through direct collision in a multiple system (Iben & Tutukov 1984; Webbink 1984; Raskin et al. 2009; Rosswog et al. 2009). This model finds explains the lack of observed hydrogen and helium lines in the late-time spectra of most SNe Ia and the delay-time distribution matches the observations well (Maoz et al. 2014). However, because the range of WD masses, about 0.7 – 1.1 M_{\odot} , which could merge to produce SNe Ia is large, the DD scenario struggles to explain the observed homogeneity of SN Ia light-curves. In addition, it is unclear whether a slow WD-WD merger produces a type Ia supernova. It is instead possible that an accretion-induced collapse forms a neutron star (Nomoto & Iben 1985).

In the SD scenario, a WD accretes material from a main-sequence

* E-mail: zwliu@ynao.ac.cn

† E-mail: r.izzard@surrey.ac.uk

‡ E-mail: kuochuan.pan@gapp.nthu.edu.tw

(MS), sub-giant (SG), red-giant (RG) or helium (He) star in a close binary system until the WD mass is close to the Chandrasekhar mass limit, M_{Ch} , at which point the star explodes as an SN Ia (Whelan & Iben 1973; Han & Podsiadlowski 2004; Liu & Stancliffe 2018, 2020). The SN ejecta-donor interaction is expected to happen naturally in the SD scenario. The thermonuclear explosion ejects the ashes at speeds of order 10^4 km s^{-1} , impacting the donor star and forcefully stripping material away from its surface, changing its structure and composition (Wheeler et al. 1975). The existence of the donor star leads to asymmetric ejecta with a cone-shaped cavity, and the ejecta-donor interaction could produce early UV flash (Kasen 2010; Liu et al. 2015; Liu & Stancliffe 2016). Additionally, the donor survives the explosion and should be identifiable by its unusual peculiar velocity. However, searches for such surviving donor stars have not yet borne fruit from the standard SD SN Ia channel (Ruiz-Lapuente et al. 2004; Ruiz-Lapuente 2019; Schaefer & Pagnotta 2012; Kerzendorf et al. 2009, 2014).

Many numerical simulations have been constructed to investigate the interaction between SN Ia ejecta and a stellar donor in the SD scenario (e.g. Marietta et al. 2000; Pakmor et al. 2008; Pan et al. 2010, 2012a; Liu et al. 2012, 2013a,b,c; Boehner et al. 2017; Bauer et al. 2019; Zeng et al. 2020), using both grid-based and smoothed particle hydrodynamics (SPH) methods. It was found that $\geq 0.1 M_{\odot}$ of hydrogen-rich material is unbound from an H-rich donor star in the SD scenario. As a result, the H lines caused by the stripped donor-star material are expected to be seen in late-time spectra of SNe Ia (Mattila et al. 2005; Botyánszki et al. 2018). However, no H/He lines have been detected in late-time spectra of normal SNe Ia (e.g., Leonard 2007; Lundqvist et al. 2015; Maguire et al. 2016; Tucker et al. 2019) and only in two rapidly-declining, subluminous events (Kollmeier et al. 2019). This poses a serious challenge to the SD scenario for SNe Ia. However, most of previous impact simulations adopt either a simplified structure and composition of the SN ejecta or use the W7 model (Nomoto et al. 1984) to represent a SN Ia explosion. This leads to uncertainty not only in the stripped-mass calculation but also in the predictions of the H-line strengths in late-time spectra of SNe Ia because the exact explosion mechanism of SNe Ia is still unknown.

A number of explosion models have been proposed to cover various progenitor scenarios of SNe Ia (Hillebrandt et al. 2013), including near Chandrasekhar-mass deflagration to detonation transitions (DDT) (Gamezo et al. 2005; Röpke et al. 2007; Khokhlov 1991; Seitenzahl et al. 2013), Chandrasekhar-mass deflagrations (Nomoto et al. 1984; Jordan et al. 2012; Kromer et al. 2013; Fink et al. 2014), gravitationally-confined detonations (Jordan et al. 2008; Seitenzahl et al. 2016), sub-Chandrasekhar-mass double detonations (Livne 1990; Woosley & Weaver 1994; Fink et al. 2007; Kromer et al. 2010; Gronow et al. 2020), violent mergers (Pakmor et al. 2010, 2011), and the collisions of two WDs (Raskin et al. 2009; Rosswog et al. 2009). Near Chandrasekhar-mass explosion models in the SD scenario have long been proposed as favourites for SNe Ia because they well reproduce some observational features such as their light curves and spectra (e.g., Hoefflich et al. 1995, 1996; Kasen et al. 2009; Blondin et al. 2011; Sim et al. 2013). The carbon deflagration model proposed by Nomoto et al. (1984), known as the W7 model, is commonly used. In this model, the ignition of carbon in the core propagates outwards as a subsonic burning front. Rayleigh-Taylor instabilities at the contact between hot ashes and cold fuel increase the surface area of the front allowing it to engulf the entire star. More recently, Seitenzahl et al. (2013) proposed a suite of three-dimensional delayed-detonation models of near Chandrasekhar-mass WDs, most notably the N100 model in which 100 ignition sparks begin the

explosion deep inside the white dwarf (Röpke et al. 2012; Seitenzahl et al. 2013). Alternatively, in the delayed-detonation model, the propagating carbon-ignition flame accelerates to a supersonic velocity, resulting in a pressure wave which causes the surrounding fuel to auto-ignite.

To use observations of type Ia supernovae to determine their origin, we must compare observations to detailed models including the ejecta-donor interaction. Modelling the explosion mechanism correctly is vital to this comparison. Therefore, in this work, we perform two-dimensional hydrodynamic simulations using two widely-studied near Chandrasekhar-mass explosion models within the SD progenitor scenario, i.e., the W7 and N100 models (Nomoto et al. 1984; Seitenzahl et al. 2013). We calculate how different explosion mechanisms alter the ejecta-donor interaction and expected observational properties, as required to place constraints on the progenitor systems and explosion mechanism of type Ia supernovae.

2 NUMERICAL METHODS AND MODELS

To investigate type Ia supernova ejecta-donor interaction in detail, we use the publicly available hydrodynamics code FLASH version 4.6¹. FLASH is a high-performance, modular, grid-based hydrodynamics framework that could be used in a wide range of physical applications (Fryxell et al. 2000). In our setup, we adopt Helmholtz equation of state (Timmer & Swesty 2000) which interpolates thermodynamic solutions from a table of the Helmholtz free energy including contributions from degenerate electrons and positrons, radiation sources and ionised particles. We use adaptive-mesh refinement (AMR) to ensure that small-scale turbulence and instabilities are resolved in locations of interest while computational time is reduced by derefining areas far from the donor star. Our grid is a 2D axisymmetric and cylindrical, centered on the donor star, with axes (r, z) .

2.1 A main-sequence donor model

The close-binary system initially consists of a MS donor star ($M_2^i = 2.5 M_{\odot}$) and a WD accretor ($M_{\text{WD}}^i = 1 M_{\odot}$), with an orbital period $P_{\text{orb}}^i = 2$ days. This is a typical SN Ia progenitor system according to the population synthesis studies of Chen et al. (2014) and Claeys et al. (2014). To create an initial donor star model we use an one-dimensional (1D) stellar evolution code, MESA (version 4906; Paxton et al. 2011, 2013, 2015, 2018). The WD is modelled as a point mass with retention efficiencies of H and He burning from Yaron et al. (2005) and Kato & Hachisu (2004), respectively. Orbital evolution, including gravitational-wave radiation and associated angular-momentum loss, is modelled as in Chen et al. (2014).

The binary system is evolved until the WD accretes enough material to reach the Chandrasekhar-mass limit ($\sim 1.4 M_{\odot}$). We show in Fig. 1 the evolution of mass transfer rate and the HR diagram of the donor star. At the time of explosion, the binary separation is $A = 6.44 R_{\odot}$, while the donor radius and mass are $R_2 = 1.68 \times 10^{11} \text{ cm}$ and $M_2 = 1.17 M_{\odot}$, respectively. The density structure of the donor star at this moment is shown in Fig. 2.

¹ <https://flash.rochester.edu/> to solve the Eulerian hydrodynamics equations in 2D cylindrical coordinates

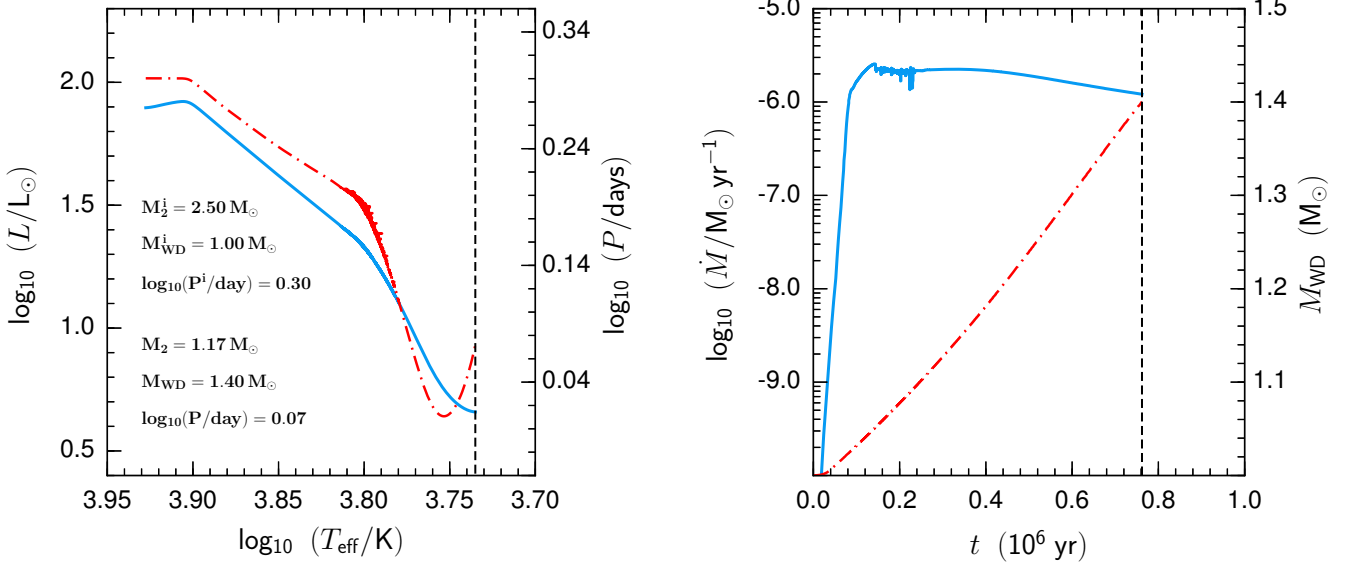


Figure 1. *Left:* Hertzsprung-Russell diagram showing change in luminosity (L , solid curve, left axis) and orbital period (P , dash-dot curve, right axis) with effective temperature. *Right:* Mass transfer rate (\dot{M} , solid curve) and white dwarf mass (M_{WD} , dash-dot curve) vs time since the start of mass transfer. In both figures the dashed vertical line represents the time of SN Ia explosion.

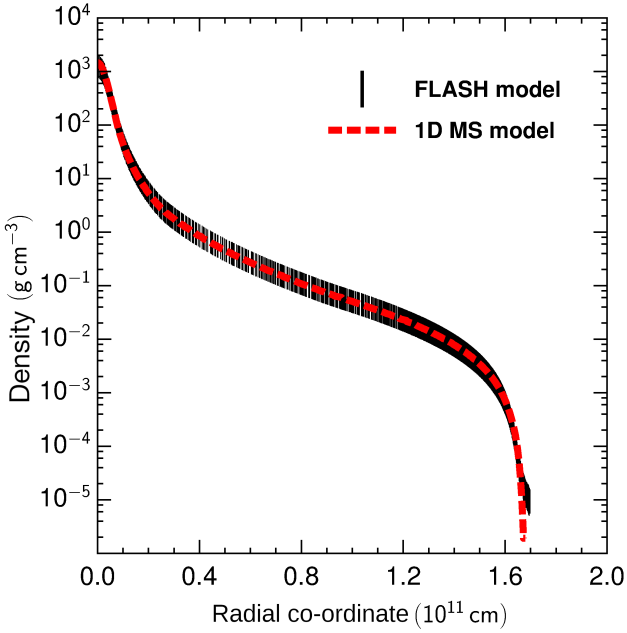


Figure 2. The radial density profile of our 1D donor model constructed with MESA (red dashed line) and its corresponding 2D FLASH model (black line) after relaxation.

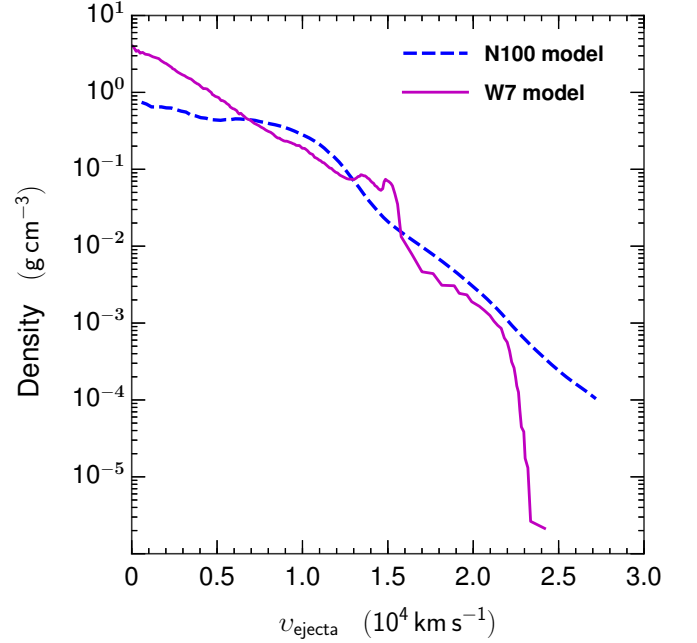


Figure 3. Density as a function of ejecta velocity in the W7 (solid line) and the N100 models (dashed line) about 100 s after the start of the explosion.

2.2 Explosion models

The W7 carbon deflagration model (Nomoto et al. 1984; Maeda et al. 2010)² and the N100 delayed-detonation model (Seitenzahl et al. 2013) are employed in this work. With both, a one-dimensional, angle-averaged shell model of the explosion 20 s after ignition is in-

terpolated onto a two-dimensional grid at the maximum refinement level of our hydrodynamical model to reduce the severity of numerical grid artifacts in the expanding gas front. Both explosions eject $1.4 M_{\odot}$ but the N100 model has a higher kinetic energy in its ejecta (1.40×10^{51} erg compared to 1.23×10^{51} erg in W7). Fig. 3 compares the density as a function of expansion velocity in N100 and W7. The N100 model also has a higher-velocity tail in the outer region of ejecta compared to W7 (see Fig. 3).

² In particular, the W7 model of Maeda et al. (2010) is used in this work.

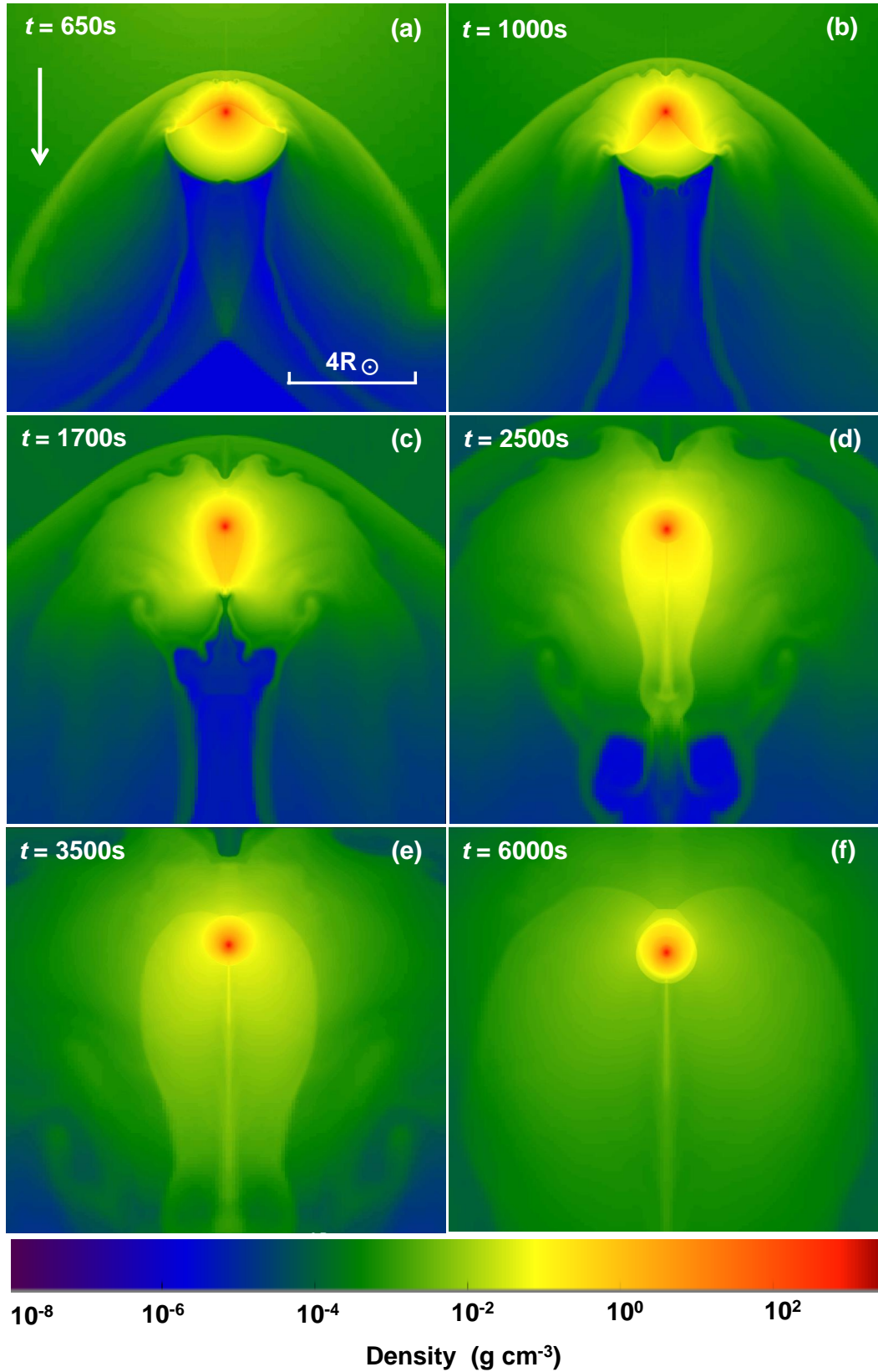


Figure 4. Density slices at times $t \approx 650\text{ s}$, 1000 s , 1700 s , 2500 s , 3500 s and 6000 s after explosion in our 2D hydrodynamical simulation of the N100 model (Seitzzahl et al. 2013). The colour scale shows the logarithm of the mass density. The direction of motion of the incoming SN ejecta is from top to bottom (see arrow symbol). The plots are made using yt (Turk et al. 2011).

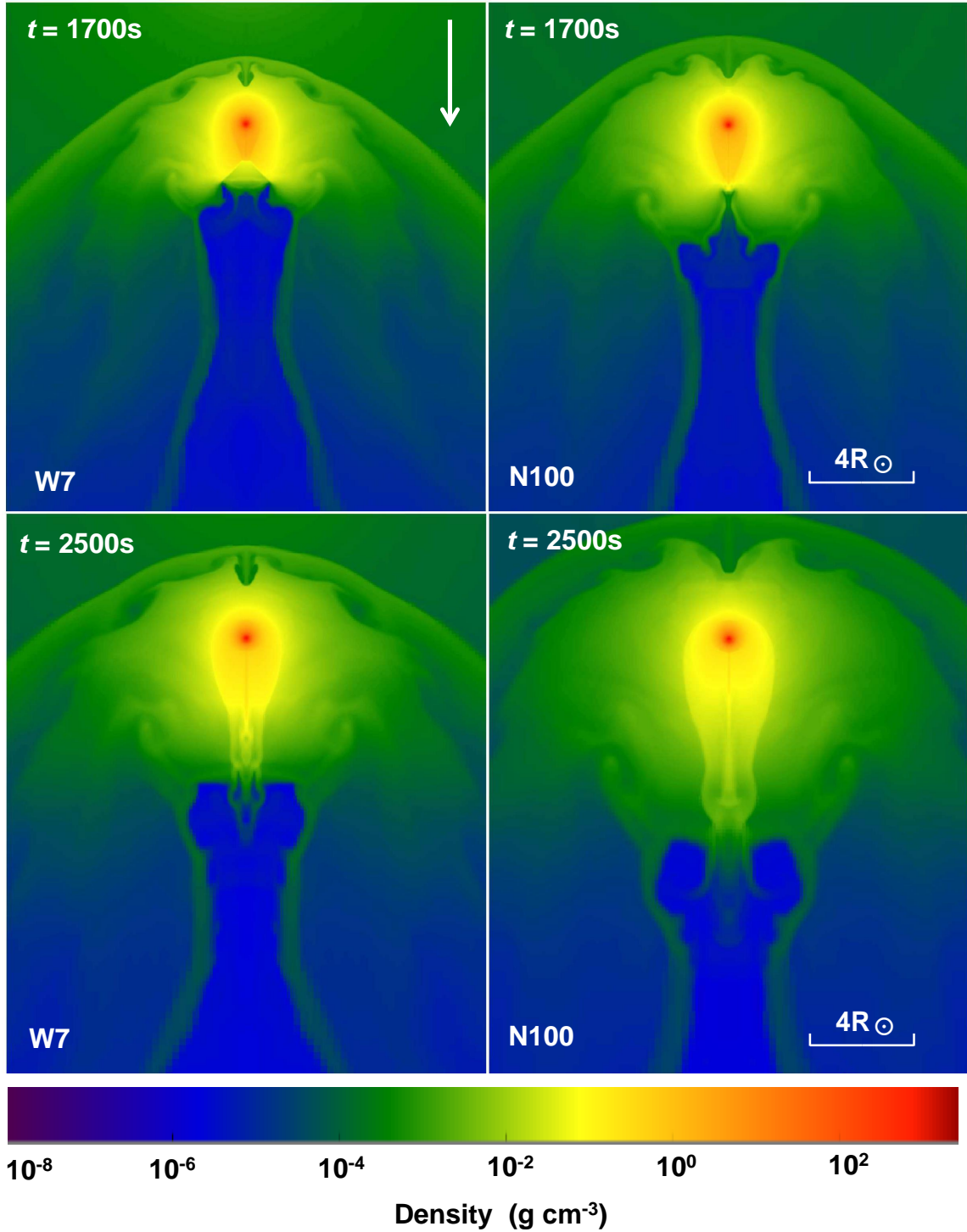


Figure 5. A comparison of density slices at $t \approx 1700$ s, 2500 s, between the W7 model (left column) and the N100 model (right column) from our 2D impact simulations. The color scale shows the logarithm of the mass density. The direction of motion of the incoming SN ejecta is from top to bottom (see arrow symbol). The plots are made by using yt (Turk et al. 2011).

2.3 Setup and key assumptions

The simulation setup is similar to what has been described in Pan et al. (2010, 2012a) but upgraded to FLASH 4 version. To initialise the hydrodynamic simulation, the MS donor-star model is interpolated onto a two-dimensional grid from the one-dimensional shell model provided by MESA. The system is then relaxed for 10^4 s which arti-

ficially damps the momentum of the star so it settles into hydrostatic equilibrium. Next, the W7 or N100 SN Ia explosion is placed at a distance A from the centre of the donor star on the z -axis. The simulation then runs for a further 10^4 s until the ejecta-donor interaction finishes and the mass of the donor star stabilises. Because the donor fills its Roche lobe at the moment of supernova, the binary separation

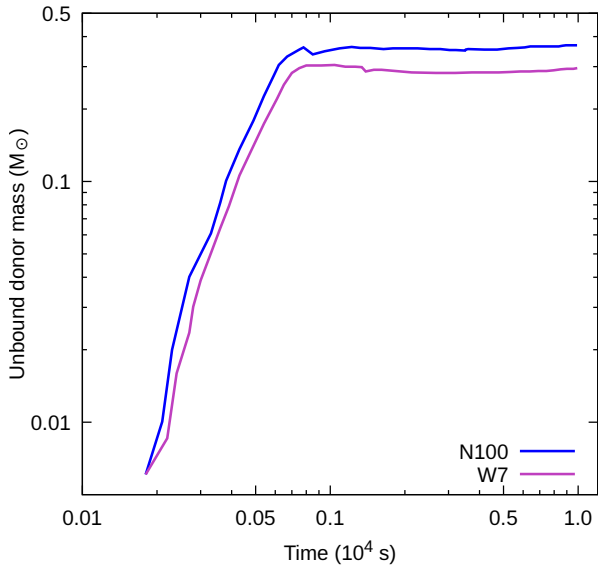


Figure 6. Unbound donor-star mass vs time since the supernova in our simulations with the W7 (dash-dotted line) and N100 (solid line) explosion models. Most mass is lost from the donor just after the blast wave shocks its surface, before about 100 s, with later thermal relaxation causing a small amount of mass to re-bind by the end of the simulation.

(A) and the donor radius (R_2) follow Equation 1 (Eggleton 1983),

$$\frac{R_2}{A} = \frac{0.49q^{2/3}}{0.6q^{2/3} + \ln(1 + q^{1/3})}, \quad (1)$$

where q is the mass ratio of binary system at the moment of explosion.

In our simulations we employ 12 levels of adaptive-mesh refinement (AMR) in the SN and donor-star regions, and a maximum of 10 levels of refinement outside these regions. We refer to this setup as the 10/12 level. This is equivalent to a uniform grid spacing of 6.1×10^7 cm ($\sim 3.6 \times 10^{-4} R_2$) inside the star and supernova regions, and a maximum of 9.8×10^6 cm ($\sim 5.8 \times 10^{-3} R_2$) outside of these regions. The cylindrical coordinates r, z lie in the ranges $r = (0, 2 \times 10^{12})$ and $z = (-2 \times 10^{12}, 2 \times 10^{12})$, which are about 12 times larger than the donor-star radius in each direction.

To determine the robustness of numerical results, Pan et al. (2010) performed a convergence test using different maximum AMR levels from 6/8 to 10/12 in their 2D impact simulations with FLASH. They found that the differences in the results, e.g. to the unbound mass and kick velocity, given by these different resolution levels are not significant, and that level 10/12 is sufficient to study ejecta-donor-star interaction. In addition, the convergence tests of Pan et al. (2010) were performed with a helium-star companion which is more compact than our main-sequence donor. The turbulence generated from ejecta-companion impact is weaker in the main-sequence channel and we expect better convergence with main-sequence companions. Because the FLASH code is used in this work, albeit a newer version, and our initial setup and assumptions are similar to those of Pan et al. (2010), we use the recommended 10/12 level in all our simulations.

We neglect orbital and rotational motion in our simulations because the SN Ia ejecta velocity ($\sim 10^4$ km s $^{-1}$) far exceeds the orbital velocity (a few $\times 10^2$ km s $^{-1}$), and the two stars are tidally locked at the time of explosion so the donor surface also rotates at the orbital velocity.

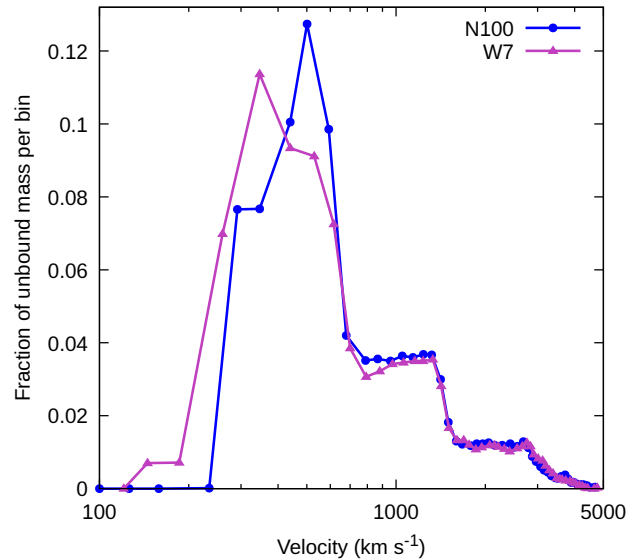


Figure 7. Velocity distributions of unbound donor-star material at end of our simulations using the two different explosion models W7 (blue dashed top-left to bottom-right) and N100 (magenta dashed bottom-left to top-right).

3 RESULTS

In this section, we present the results of our 2D hydrodynamical simulations of ejecta-companion interaction, including the stripped mass and kick velocity. A comparison of the results between W7 model and N100 model is given to discuss the effect of different explosion models on the details of ejecta-companion interaction.

3.1 Ejecta-donor interaction

Fig. 4 shows the evolution of the ejecta-donor interaction in our N100 model. The exploding star is located vertically above the figure, out of shot, and the blast wave moves downwards towards the donor. The SN ejecta expands freely for a few minutes then hits the surface of the donor star. The impact strips some H-rich material from and increases the pressure on the surface of the donor. A high-pressure shock is driven into the stellar interior and a bow shock develops in the outer regions which diverts SN ejecta material around the star. As the diverted material further expands around the donor star, the interstellar medium (ISM) is compressed in the downstream region (below the star in the figure). The two opposing fronts collide behind the star at a few hundred seconds (Fig. 4a), forcing ISM material back towards the star, whose impact can be observed as a small notch at its rear. The shock continues to pass through the donor star, slowing as it moves through the higher density core (Fig. 4b). The opening hole is created behind the donor star.

Instabilities develop on the donor surface closest to the SN, disrupting its initially-spherical shape. At about $t = 1700$ s the shock passes through the entire star and pushes stellar material out of its rear as it exits (Fig. 4c). The symmetries of the donor star are completely destroyed as the shock passes through it. The stripped donor material mixes with the SN ejecta material in the opening hole behind the star (Fig. 4d). The outer layers of the star expand in the shape of an inverted teardrop, surrounded by Rayleigh-Taylor instabilities. Instabilities are also observed at the edge closest to the SN, travelling

outwards from the centre of the donor but shielded from incoming material by a bow shock. The donor star expands because of the shock heating, and is totally out of hydrostatic and thermal equilibrium. By $t = 6000$ s, the donor starts returns to hydrostatic equilibrium as the interaction finishes and a relatively spherical remnant remains (Fig. 4f). At the same time, an expanded low-density envelope has forms in the outer region of the star. In addition, the centre of the donor star moves away from its original position because it receives a velocity kick because of momentum imparted by the SN ejecta during the interaction.

3.2 Stripped mass and kick velocity

A comparison of the interaction between the W7 and N100 explosion models at equal times after the supernova explosion is shown in Fig. 5. Both explosion models lead to similar interaction characteristics: a turbulent front behind the frontal bow shock, eddies to the sides of the rear of the star, and the teardrop-shaped plume ejected after the shock passes through the star in its entirety. The clearest difference is that the N100 explosion has faster ejecta, hence the interaction evolves more quickly than with W7 and strips more material from the donor star.

Fig. 6 shows the unbound donor mass as a function of time using the two explosion models in our simulations. To determine whether the donor material is unbound, we calculate its total energy by summing the kinetic, potential and internal energies, $E_{\text{tot}} = E_{\text{kin}} + E_{\text{pot}} + E_{\text{int}}$, and if $E_{\text{tot}} > 0$ the material is unbound. As shown in Fig. 6, the unbound donor mass stabilises about 5000 s after the explosion. The time-evolution of unbound mass is similar in both models, beginning with a steep rise as the shock front transfers momentum and thermal energy to the donor star, followed by a slight decrease during thermal relaxation which returns some material to a bound state. At the end of our simulations, we find that $0.293 M_{\odot}$ and $0.368 M_{\odot}$ of H-rich material, representing 25 and 31 per cent of the donor mass at the time of explosion, is stripped from the MS donor surface by the SN explosion using the W7 and N100 models respectively.

Extra mass stripping in our N100 model is caused by the larger kinetic energy of the N100 explosion, 1.40×10^{51} erg (Seitenzahl et al. 2013), compared with W7 which has 1.23×10^{51} erg (Nomoto et al. 1984). Previous studies have found that more powerful ejecta generally strip more donor mass for a given donor model and binary separation, and the total stripped mass is linearly proportional to the SN kinetic energy (Pakmor et al. 2008; Pan et al. 2012a; Liu et al. 2013a). The stripped mass in our W7 model increases to $0.334 M_{\odot}$ if we scale it with a higher kinetic energy of 1.40×10^{51} erg. On the other hand, as shown in Fig. 3, the outer SN ejecta of the N100 model is more powerful than that of W7, hence N100 is also expected to strip more.

As described in Section 1, the interaction between SN Ia ejecta and a donor star has been investigated by previous studies with both analytical methods, and two- and three-dimensional hydrodynamical simulations (e.g., Wheeler et al. 1975; Marietta et al. 2000; Pakmor et al. 2008; Pan et al. 2012a; Liu et al. 2012; Boehner et al. 2017). Most studies found that $\gtrsim 0.1 M_{\odot}$ can be stripped from a main-sequence donor star, from a red giant the whole envelope is stripped. In particular, Marietta et al. (2000) found that 15 per cent of the donor star is stripped in their HCV model. The HCV model has a mass $M_2 = 1.017 M_{\odot}$, radius $R_2 = 6.8 \times 10^{10}$ cm and ratio of binary separation to radius $A/R_2 = 3.0$ (Marietta et al. 2000). Compared to our main-sequence donor model, the HCV model is more compact and has a larger A/R_2 (Table 1). The stripped mass in HCV increases

to $\sim 0.2 M_{\odot}$ (Pan et al. 2012a, see their Fig. 12) if we reduce its A/R_2 to 2.67 similarly to our model. Liu et al. (2012) found between 6 and 24 per cent depending on the MS donor model (see also Pan et al. 2012a). More recently, Boehner et al. (2017) predicted 21 – 26 per cent of a main-sequence donor is stripped in their 2D simulations using FLASH. Our results are comparable with these previous studies. As shown in Figs. 2 and 1, our donor star is near the end of its main sequence at the time of SN explosion, hence it has a dense core with an extended envelope. This explains why our stripped mass is a greater than in Boehner et al. (2017), in which the donor stars are normal MS stars and they have a more compact envelope than our donor model. However, our stripped mass greatly exceeds the ~ 1 –5 per cent predictions of Pakmor et al. (2008, their Table 2). The differences are mainly caused by the detailed structure of the donor star models and binary separations at the moment of SN Ia explosion (Liu et al. 2012; Pan et al. 2012a; Boehner et al. 2017).

Compared to our model, the main-sequence donor models of Pakmor et al. (2008) are more compact and have longer binary separations (i.e., they have a larger A/R_2) so in their simulations less mass is stripped. For instance, model rp3_24a in Pakmor et al. (2008) has a binary separation of 4.39×10^{11} cm which is similar to our 4.48×10^{11} cm. However, our companion radius exceeds theirs (7.21×10^{10} cm) by a factor of 2.3. Additionally, model rp3_20a in Pakmor et al. (2008) has the same mass as ours (i.e., $M_2 = 1.17 M_{\odot}$), but their $A/R_2 = 4.5$ exceeds ours ($A/R_2 = 2.67$) by a factor of 1.7. If we assume that their rp3_20a model also has $A/R_2 = 2.67$, their stripped mass increases to $0.19 M_{\odot}$ based on their Equation 4. The main differences between the main-sequence donor models of Pakmor et al. (2008) and ours are the different treatments of pre-SN mass-loss of the MS stars and the binary separations adopted at the moment of SN explosion, which have been discussed in detail in our previous work (Liu et al. 2012, their Section 4.1). Pakmor et al. (2008) start the mass accretion phase with less-evolved companion stars and they constructed their companion star models by rapidly removing mass while evolving a single main-sequence star to mimic pre-SN mass-transfer in a binary system. As a consequence, their models have a very large A/R_2 , and they are too compact to fill their Roche-lobe at the moment of SN explosion. In contrast, our main-sequence donor model is constructed by consistently following mass-transfer in a binary system. Our main-sequence star has a more extended structure and fills its Roche-lobe when the SN explodes.

The donor star receives a kick as a result of momentum transfer from the ejecta during the interaction. The time evolution of kick velocity behaves similarly to the stripped mass (Fig. 6). At the end of simulations ($t = 10^4$ s), the kick velocities are 73.8 km s^{-1} and 86.0 km s^{-1} in our W7 and N100 models respectively. The faster kick in the N100 model is probably because its ejecta have a higher kinetic energy than in W7. The movement of the donor away from its original position is seen in Fig. 4. The final spatial velocity of the surviving donor star is only slightly altered by the kick, with most of the velocity arising from its pre-explosion orbital motion.

4 DISCUSSION

In this section, we compare our results with the late-time observations of SNe Ia to examine the validity of the SD progenitor model. In addition, we discuss the distributions of stripped companion material and the properties of surviving companion stars to derive some clues to the identification of SD progenitor model. Uncertainties in our results and future work are also given.

Table 1. Parameters summarising our initial models and results.

Simulation	SN model	$E_{\text{kin,SN}}$ (10^{51} erg)	M_{WD}^i (M_{\odot})	M_2^i (M_{\odot})	M_2 (M_{\odot})	R_2 (10^{11} cm)	A (10^{11} cm)	$\Delta M_{\text{stripped}}$ (M_{\odot})	V_{kick} (km s^{-1})	V_{modal} (km s^{-1})
A	W7	1.23	1.000	2.500	1.170	1.68	4.48	0.293	73.8	350
B	N100	1.40	1.000	2.500	1.170	1.68	4.48	0.368	86.0	500

$E_{\text{kin,SN}}$ is the kinetic energy of SN ejecta of the explosion model. M_{WD}^i and M_2^i are the WD and donor masses at the beginning of mass transfer. M_2 , R_2 and A are the donor mass, donor radius and binary separation at the time of explosion. $\Delta M_{\text{stripped}}$ and V_{kick} are the mass stripped from the donor and the kick velocity received by the donor star at the end of our 2D impact simulations. V_{modal} is the typical velocity of stripped donor material (Fig. 7).

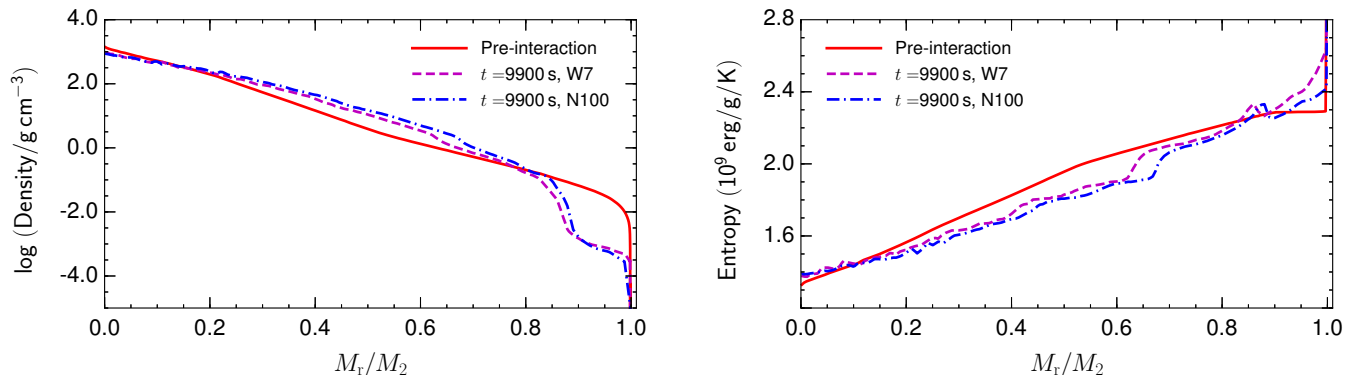


Figure 8. Post-impact 1D averaged density (left panel) and entropy (right panel) of the surviving donor star as a function of relative mass, M_r/M_2 where M_r is the Lagrangian mass co-ordinate, at the end of our simulations, when $t \approx 10^4$ s, with the W7 (red dashed line) and N100 (green dash-dotted line) explosion models. For comparison, the corresponding 1D profiles of initial pre-impact donor star are also shown as solid lines.

4.1 Models compared to observations

Hydrogen-emission lines will be seen in late-time spectra of SNe Ia, about a few hundred days after the explosion, if sufficient hydrogen-rich material ($> 0.001 - 0.058 M_{\odot}$, which depends on the distance of the observed SNe Ia) is stripped from the donor surface during the interaction of the explosion with the star (Mattila et al. 2005; Lundqvist et al. 2015; Botyánszki et al. 2018; Dessart et al. 2020). Therefore, searching for hydrogen-emission lines in late-time spectra of SNe Ia should provide strong evidence in favour, or otherwise, of a SD progenitor system to observed Ia supernovae. To date, no hydrogen-emission lines have been detected in late-time spectra of normal SNe Ia (Leonard 2007; Lundqvist et al. 2013, 2015; Maguire et al. 2016; Shappee et al. 2016; Tucker et al. 2020). However, hydrogen features have been detected in late-time spectra of two fast-declining, sub-luminous SNe Ia, SN 2018fhw (Kollmeier et al. 2019) and SN 2018cuj (Prieto et al. 2020). All this late-time observations limit the hydrogen-rich mass in type-Ia SN progenitor systems to $\leq 0.001 - 0.058 M_{\odot}$.

This observational upper limit to the stripped mass is less than our simulations predict, $\geq 0.30 M_{\odot}$, and our results are similar to previous studies (Marietta et al. 2000; Pakmor et al. 2008; Pan et al. 2012a; Liu et al. 2012; Liu & Stancliffe 2017; Boehner et al. 2017). This suggests that the non-detection of hydrogen features in late-time spectra of SNe Ia is seriously challenges the SD scenario if we assume that our current hydrodynamical and radiative transfer models of late-time hydrogen emission are accurate.

4.2 Velocity distributions of stripped material

The distribution of velocities of H/He-rich material stripped from the donor star hints at expected H- and He-emission line features in late-time spectra of SNe Ia (Mattila et al. 2005; Botyánszki et al. 2018; Dessart et al. 2020). In Fig. 7, we show post-impact velocity distributions of stripped material from the surface of our donor star in our two explosion models. The typical velocities of stripped material in our W7 and N100 models are 350 km s^{-1} and 500 km s^{-1} , respectively, which are consistent with previous works (Marietta et al. 2000; Pan et al. 2012a; Liu et al. 2012).

Additionally, Marietta et al. (2000) suggests that the high-velocity tail of stripped material is an important diagnostic that allows discrimination between various donor models (see also Boehner et al. 2017). Here, we check whether the two explosion models investigated in this work can be discriminated similarly. Fig. 7 shows that although a high-velocity, $\geq 1000 \text{ km s}^{-1}$, tail is seen in both our explosions models, there is little difference between their velocity distributions. This suggests that it may be difficult to discriminate between the W7 and N100 models with the features caused by the high-velocity tail for a given main-sequence donor star model.

4.3 Surviving donor stars

In the SD SNIa scenario, the donor star survives the explosion after ejecta-donor interaction. However, surviving donor stars are generally not expected in the double-degenerate scenario, although Shen et al. (2018) have recently suggested that a WD donor may survive in their D6 double-generate model. Therefore, searching for surviving

donor stars in SN remnants (SNRs) is a promising way to distinguish between the SD and DD scenarios of SNe Ia (Ruiz-Lapuente et al. 2004; Ruiz-Lapuente 2019; Kerzendorf et al. 2009, 2013; Schaefer & Pagnotta 2012; Pan et al. 2014; Li et al. 2019).

To provide the predicted observational features of surviving donor stars for comparison with observations of SNRs, it is important to address long-term post-impact evolution of surviving donor stars based on the results of multi-dimensional hydrodynamical impact simulations. After the explosion, the surviving donor star becomes a runaway star. It escapes from the binary system with a spatial velocity caused mostly by its pre-explosion orbital motion. In Figure 8, we present 1D-averaged density (left panel) and entropy (right panel) profiles of our surviving main-sequence donor star at the end of our simulations with the W7 and N100 explosions. For comparison, the initial profiles of the donor star at the beginning of the simulations are also shown. The central density of the donor star decreases by about 50 per cent because of the shock that passes through the star. In addition, the donor star is impacted and heated during the interaction, and expands by a factor of about two by the end of our simulations.

While the donor subsequently thermally relaxes, it is overluminous compared to its pre-explosion equilibrium state (Podsiadlowski 2003; Pan et al. 2012b, 2013; Shappee et al. 2013; Liu & Zeng 2020; Liu et al. 2021, 2022). For instance, Pan et al. (2012a) and Shappee et al. (2013) suggest that the post-impact main-sequence companion stars are significantly more luminous (up to about 10–1000 L_{\odot}) within a few thousand years, depending on the main-sequence companion model. Using the approach of Liu & Zeng (2020), the 2D surviving donor model computed from our impact simulations in this work can be mapped into a 1D stellar evolution code such as MESA to follow their subsequent post-impact evolution for more than a few hundred years to obtain expected observational features (Pan et al. 2013; Liu et al. 2021, 2022). This is important to understand how different explosion models affect the observational features of the surviving main-sequence companion stars, and is useful in the search for such events in SN Ia remnants. This investigation will be performed in a forthcoming study.

4.4 Uncertainties and future work

Our simulations are performed in 2D without considering the orbital motion and rotation of the binary system. This is expected to only slightly affect our results (Liu et al. 2012; Pan et al. 2012a) because these two velocities are slower than the typical ejecta velocity of 10^4 km s^{-1} by more than an order of magnitude. Pan et al. (2012a) have performed the ejecta-donor interaction in 2D and 3D for a given main-sequence donor model with the FLASH code. They find that the results of the ejecta-donor interaction are quite consistent in 2D and 3D if the orbital motion and spin of the star are not included. However, the orbital motion and spin can lead to slightly different results in 3D (Pan et al. 2012a, their Table 2). Future 3D simulations are still needed to make more strict theoretical predictions such as post-SN rotation features of the surviving donor star. For instance, exploring the post-impact spin features of the surviving donor star requires the impact simulation to be in 3D.

In addition, the rotation of an accreting WD is not considered when we construct the donor model at the moment of SN explosion in our 1D binary evolution calculation. The accretion from the donor star spins up the WD, leading to a delay to spin down the WD before it explodes (i.e., the so-called “spin up/spin down” model, Justham 2011; Di Stefano et al. 2011). Because the spin-down timescale is quite uncertain, the donor star in the MS donor scenario could be any type of star from MS (short delay) to WD (long delay) at the time

of explosion. In such a case, the amount of stripped donor mass and donor properties will very likely differ considerably from our results with a MS donor.

5 SUMMARY AND CONCLUSIONS

In this work, the effects of different explosions on the results of the ejecta-donor interaction in normal SNe Ia are investigated with 2D hydrodynamical simulations using the FLASH code for a given MS donor which is computed by the MESA code. Specifically, two near-Chandrasekhar mass explosion models, W7 (Nomoto et al. 1984) and N100 (Röpke et al. 2012; Seitenzahl et al. 2013), are adopted to represent the SN Ia explosion in our simulations. The main goal of this work is to investigate how different explosion models affect the results of ejecta-donor interaction such as the total amount of stripped donor material and the kick velocity received by the donor star during the interaction. We find that $0.30 M_{\odot}$ and $0.37 M_{\odot}$ are stripped from a typical $2.5 M_{\odot}$ main-sequence donor surface by the SN Ia explosion, in simulations with the W7 and N100 explosion models, respectively. Additionally, the donor star receives a kick velocity of about 74 km s^{-1} and 86 km s^{-1} , respectively. The modal velocity ($\sim 500 \text{ km s}^{-1}$) of stripped material in the N100 model exceeds that of the W7 model ($\sim 350 \text{ km s}^{-1}$) by a factor of 1.4. We therefore conclude that our numerical results of ejecta-donor interaction are not significantly dependent on the studied two near-Chandrasekhar-mass explosion models.

ACKNOWLEDGEMENTS

We thank the anonymous referee for their comments that helped to improve this paper. CM thanks the University of Surrey and Yunnan Observatories for their guidance and support during his foreign-exchange year. ZWL is supported by the National Natural Science Foundation of China (NSFC, Nos. 11873016, 11973080, and 11733008), the National Key R&D Program of China (Nos. 2021YFA1600400, 2021YFA1600401), the Chinese Academy of Sciences, Yunnan Fundamental Research Projects (Grant No. 202001AW070007) and Yunnan Province (Nos. 12090040, 12090043, 2019HA012, and 2017HC018) and thanks the University of Surrey *Institute of Advanced Studies* for a visiting fellowship. RGI was supported by STFC grants ST/L003910/1 and ST/R000603/1, and thanks Yunnan Observatories for their gracious hospitality during exchange visits. KCP is supported by the Ministry of Science and Technology of Taiwan through grants MOST 107-2112-M-007-032-MY3 and MOST 110-2112-M-007-019. HLC is supported by the National Natural Science Foundation of China (NSFC, Nos. 12073071) and Yunnan Fundamental Research Projects (Grant Nos. 202001AT070058, 202101AW070003), the science research grants from the China Manned Space Project with No. CMS-CSST-2021-A10 and Youth Innovation Promotion Association of Chinese Academy of Sciences (Grant no. 2018076). The authors gratefully acknowledge the “PHOENIX Supercomputing Platform” jointly operated by the Binary Population Synthesis Group and the Stellar Astrophysics Group at Yunnan Observatories, CAS. This work made use of the Heidelberg Supernova Model Archive (HESMA, <https://hesma.h-its.org>, Kromer et al. 2017).

DATA AVAILABILITY

The data underlying this article will be shared on reasonable request to the corresponding author.

REFERENCES

- Bauer E. B., et al., 2019, *ApJ*, **887**, 68
- Blondin S., Kasen D., Röpke F. K., Kirshner R. P., Mandel K. S., 2011, *MNRAS*, **417**, 1280
- Boehner P., Plewa T., Langer N., 2017, *MNRAS*, **465**, 2060
- Botyánszki J., Kasen D., Plewa T., 2018, *ApJ*, **852**, L6
- Chen H.-L., Woods T. E., Yungelson L. R., Gilfanov M., Han Z., 2014, *MNRAS*, **445**, 1912
- Claeys J. S. W., Pols O. R., Izzard R. G., Vink J., Verbunt F. W. M., 2014, *A&A*, **563**, A83
- Dessart L., Leonard D. C., Prieto J. L., 2020, *A&A*, **638**, A80
- Di Stefano R., Voss R., Claeys J. S. W., 2011, *ApJ*, **738**, L1
- Eggleton P. P., 1983, *ApJ*, **268**, 368
- Fink M., Hillebrandt W., Röpke F. K., 2007, *A&A*, **476**, 1133
- Fink M., et al., 2014, *MNRAS*, **438**, 1762
- Fryxell B., et al., 2000, *ApJS*, **131**, 273
- Gamezo V. N., Khokhlov A. M., Oran E. S., 2005, *ApJ*, **623**, 337
- Gronow S., Collins C., Ohlmann S. T., Pakmor R., Kromer M., Seitzzahl I. R., Sim S. A., Röpke F. K., 2020, arXiv e-prints, p. arXiv:2002.00981
- Han Z., Podsiadlowski P., 2004, *MNRAS*, **350**, 1301
- Hillebrandt W., Kromer M., Röpke F. K., Ruiter A. J., 2013, *Frontiers of Physics*, **8**, 116
- Hoeflich P., Khokhlov A. M., Wheeler J. C., 1995, *ApJ*, **444**, 831
- Hoeflich P., Khokhlov A., Wheeler J. C., Phillips M. M., Suntzeff N. B., Hamuy M., 1996, *ApJ*, **472**, L81
- Hoyle F., Fowler W. A., 1960, *ApJ*, **132**, 565
- Iben Jr. I., Tutukov A. V., 1984, *ApJ*, **284**, 719
- Jordan G. C. I., Fisher R. T., Townsley D. M., Calder A. C., Graziani C., Asida S., Lamb D. Q., Truran J. W., 2008, *ApJ*, **681**, 1448
- Jordan IV G. C., Perets H. B., Fisher R. T., van Rossum D. R., 2012, *ApJ*, **761**, L23
- Justham S., 2011, *ApJ*, **730**, L34+
- Kasen D., 2010, *ApJ*, **708**, 1025
- Kasen D., Röpke F. K., Woosley S. E., 2009, *Nature*, **460**, 869
- Kato M., Hachisu I., 2004, *ApJ*, **613**, L129
- Kerzendorf W. E., Schmidt B. P., Asplund M., Nomoto K., Podsiadlowski P., Frebel A., Fesen R. A., Yong D., 2009, *ApJ*, **701**, 1665
- Kerzendorf W. E., et al., 2013, *ApJ*, **774**, 99
- Kerzendorf W. E., Childress M., Scharwächter J., Do T., Schmidt B. P., 2014, *ApJ*, **782**, 27
- Khokhlov A. M., 1991, *A&A*, **245**, 114
- Kollmeier J. A., et al., 2019, *MNRAS*, **486**, 3041
- Kromer M., Sim S. A., Fink M., Röpke F. K., Seitzzahl I. R., Hillebrandt W., 2010, *ApJ*, **719**, 1067
- Kromer M., et al., 2013, *MNRAS*, **429**, 2287
- Kromer M., Ohlmann S., Röpke F. K., 2017, *Mem. Soc. Astron. Italiana*, **88**, 312
- Leonard D. C., 2007, *ApJ*, **670**, 1275
- Li C.-J., et al., 2019, *ApJ*, **886**, 99
- Liu Z.-W., Stancliffe R. J., 2016, *MNRAS*, **459**, 1781
- Liu Z.-W., Stancliffe R. J., 2017, *MNRAS*, **470**, L72
- Liu Z.-W., Stancliffe R. J., 2018, *MNRAS*, **475**, 5257
- Liu Z., Stancliffe R. J., 2020, *A&A*, **641**, A20
- Liu Z.-W., Zeng Y., 2020, *MNRAS*,
- Liu Z. W., Pakmor R., Röpke F. K., Edelmann P., Wang B., Kromer M., Hillebrandt W., Han Z. W., 2012, *A&A*, **548**, A2
- Liu Z.-W., Pakmor R., Röpke F. K., Edelmann P., Hillebrandt W., Kerzendorf W. E., Wang B., Han Z. W., 2013a, *A&A*, **554**, A109
- Liu Z.-W., et al., 2013b, *ApJ*, **774**, 37
- Liu Z.-W., Kromer M., Fink M., Pakmor R., Röpke F. K., Chen X. F., Wang B., Han Z. W., 2013c, *ApJ*, **778**, 121
- Liu Z.-W., Moriya T. J., Stancliffe R. J., 2015, *MNRAS*, **454**, 1192
- Liu Z.-W., Röpke F. K., Zeng Y., Heger A., 2021, *A&A*, **654**, A103
- Liu Z.-W., Röpke F. K., Zeng Y., 2022, *ApJ*, **928**, 146
- Livne E., 1990, *ApJ*, **354**, L53
- Lundqvist P., et al., 2013, *MNRAS*, **435**, 329
- Lundqvist P., et al., 2015, *A&A*, **577**, A39
- Maeda K., Röpke F. K., Fink M., Hillebrandt W., Travaglio C., Thielemann F. K., 2010, *ApJ*, **712**, 624
- Maguire K., Taubenberger S., Sullivan M., Mazzali P. A., 2016, *MNRAS*, **457**, 3254
- Maoz D., Mannucci F., Nelemans G., 2014, *ARA&A*, **52**, 107
- Marietta E., Burrows A., Fryxell B., 2000, *ApJS*, **128**, 615
- Mattila S., Lundqvist P., Sollerman J., Kozma C., Baron E., Fransson C., Leibundgut B., Nomoto K., 2005, *A&A*, **443**, 649
- Nomoto K., Iben Jr. I., 1985, *ApJ*, **297**, 531
- Nomoto K., Thielemann F.-K., Yokoi K., 1984, *ApJ*, **286**, 644
- Pakmor R., Röpke F. K., Weiss A., Hillebrandt W., 2008, *A&A*, **489**, 943
- Pakmor R., Kromer M., Röpke F. K., Sim S. A., Ruiter A. J., Hillebrandt W., 2010, *Nature*, **463**, 61
- Pakmor R., Hachinger S., Röpke F. K., Hillebrandt W., 2011, *A&A*, **528**, A117+
- Pan K.-C., Ricker P. M., Taam R. E., 2010, *ApJ*, **715**, 78
- Pan K.-C., Ricker P. M., Taam R. E., 2012a, *ApJ*, **750**, 151
- Pan K.-C., Ricker P. M., Taam R. E., 2012b, *ApJ*, **760**, 21
- Pan K.-C., Ricker P. M., Taam R. E., 2013, *ApJ*, **773**, 49
- Pan K.-C., Ricker P. M., Taam R. E., 2014, *ApJ*, **792**, 71
- Paxton B., Bildsten L., Dotter A., Herwig F., Lesaffre P., Timmes F., 2011, *ApJS*, **192**, 3
- Paxton B., et al., 2013, *ApJS*, **208**, 4
- Paxton B., et al., 2015, *ApJS*, **220**, 15
- Paxton B., et al., 2018, *ApJS*, **234**, 34
- Perlmutter S., et al., 1999, *ApJ*, **517**, 565
- Podsiadlowski P., 2003, arXiv:astro-ph/0303660,
- Prieto J. L., et al., 2020, *ApJ*, **889**, 100
- Raskin C., Timmes F. X., Scannapieco E., Diehl S., Fryer C., 2009, *MNRAS*, **399**, L156
- Riess A. G., et al., 1998, *AJ*, **116**, 1009
- Röpke F. K., Hillebrandt W., Schmidt W., Niemeyer J. C., Blinnikov S. I., Mazzali P. A., 2007, *ApJ*, **668**, 1132
- Röpke F. K., et al., 2012, *ApJ*, **750**, L19
- Rosswog S., Kasen D., Guillochon J., Ramirez-Ruiz E., 2009, *ApJ*, **705**, L128
- Ruiz-Lapuente P., 2019, *New Astron. Rev.*, **85**, 101523
- Ruiz-Lapuente P., et al., 2004, *Nature*, **431**, 1069
- Schaefer B. E., Pagnotta A., 2012, *Nature*, **481**, 164
- Schmidt B. P., et al., 1998, *ApJ*, **507**, 46
- Seitzzahl I. R., et al., 2013, *MNRAS*, **429**, 1156
- Seitzzahl I. R., et al., 2016, *A&A*, **592**, A57
- Shappee B. J., Kochanek C. S., Stanek K. Z., 2013, *ApJ*, **765**, 150
- Shappee B. J., Piro A. L., Stanek K. Z., Patel S. G., Margutti R. A., Lipunov V. M., Pogge R. W., 2016, preprint, (arXiv:1610.07601)
- Shen K. J., Kasen D., Weinberg N. N., Bildsten L., Scannapieco E., 2010, *ApJ*, **715**, 767
- Shen K. J., et al., 2018, *ApJ*, **865**, 15
- Sim S. A., Röpke F. K., Hillebrandt W., Kromer M., Pakmor R., Fink M., Ruiter A. J., Seitzzahl I. R., 2010, *ApJ*, **714**, L52
- Sim S. A., et al., 2013, *MNRAS*, **436**, 333
- Taam R. E., 1980, *ApJ*, **242**, 749
- Timmes F. X., Swesty F. D., 2000, *ApJS*, **126**, 501
- Tucker M. A., et al., 2019, *MNRAS*, p. 3025
- Tucker M. A., et al., 2020, *MNRAS*, **493**, 1044
- Turk M. J., Smith B. D., Oishi J. S., Skory S., Skillman S. W., Abel T., Norman M. L., 2011, *ApJS*, **192**, 9
- Webbink R. F., 1984, *ApJ*, **277**, 355
- Wheeler J. C., Lecar M., McKee C. F., 1975, *ApJ*, **200**, 145
- Whelan J., Iben Jr. I., 1973, *ApJ*, **186**, 1007
- Woosley S. E., Kasen D., 2011, *ApJ*, **734**, 38
- Woosley S. E., Weaver T. A., 1994, *ApJ*, **423**, 371
- Yaron O., Prialnik D., Shara M. M., Kovetz A., 2005, *ApJ*, **623**, 398

Zeng Y., Liu Z.-W., Han Z., 2020, [ApJ](#), 898, 12